Acta Crystallographica Section D
Biological Crystallography
ISSN 0907-4449

Structure of an acidic phospholipase A_2 from the venom of *Deinagkistrodon acutus*

Lichuan Gu,[a] Hailong Zhang,[a] Shiying Song,[a] Yuancong Zhou[b] and Zhengjiong Lin[a]*

[a]National Laboratory of Biomacromolecules, Institute of Biophysics, Chinese Academy of Sciences, Beijing 100101, People's Republic of China, and [b]Institute of Biochemistry and Cell Biology, Chinese Academy of Sciences, Shanghai 200031, People's Republic of China

Correspondence e-mail: lin@sun5.ibp.ac.cn

Received 9 July 2001
Accepted 25 October 2001

PDB Reference: acidic phospholipase A_2, 1ijl.

An acidic phospholipase A_2 was purified from *Deinagkistrodon acutus* (*Agkistrodon acutus*) which displays an inhibitory effect on platelet aggregation. The three-dimensional structure of the enzyme was determined by molecular replacement at 2.6 Å resolution with a crystallographic R factor of 18.40% (R_{free} = 22.50%) and reasonable stereochemistry. Two molecules in the asymmetric unit form a dimer and the dimer formation accompanies a significant conformational adaptation of segment 14–23, a constituent of the 'interface recognition site' (IRS). This probably reflects the inherent structural flexibility of the IRS. The possible expansion of the site for inhibiting platelet aggregation as proposed previously [Wang *et al.* (1996), *J. Mol. Biol.* **255**, 669–676] is discussed.

1. Introduction

Phospholipase A_2 (PLA_2; E.C. 3.1.1.4) catalyzes the hydrolysis of the fatty acid ester at the *sn*-2 position of phospholipids in a calcium-dependent reaction. The secretory PLA_2s are classified into two main groups based on sequence and structural homology. In addition to being a catalyst for the hydrolysis of phospholipids, PLA_2s from snake venoms possess a wide variety of pharmacological activities (Gowda *et al.*, 1994; Betzel *et al.*, 1999) such as neurotoxicity, haemolytic activity, cardiotoxicity, myotoxicity and anticoagulant and antiplatelet activities.

The activity of phospholipase A_2 on substrates presenting multimolecular aggregates has long been known to be two or three orders of magnitude higher than on monomolecular dispersed molecules (interfacial activation). Large numbers of studies focusing on this phenomenon have produced two complementary theories (Derewenda, 1995). The 'substrate theory' states that the substrate properties are responsible for the phenomenon (Wells *et al.*, 1974; Scott, White *et al.*, 1990; Peters *et al.*, 1995). The 'enzyme theory' argues that phospholipase A_2 undergoes a significant conformational change (allosteric activity) when binding to an oil/water interface (van den Berg, Tessari, Boelens, Dijkman, de Haas *et al.*, 1995; Berg *et al.*, 1997).

The molecular mechanism behind this activation has been investigated for free PLA_2s as well as PLA_2 complexes using both NMR (van den Berg, Tessari, Boelens, Dijkman, de Haas *et al.*, 1995; van den Berg, Tessari, Boelens, Dijkman, Kaptein *et al.*, 1995; van den Berg, Tessari, de Haas *et al.*, 1995; Jerala *et al.*, 1996; Yuan *et al.*, 1999) and X-ray crystallographic methods (Scott, Otwinowski *et al.*, 1990; Scott, White *et al.*, 1990; Dijkstra *et al.*, 1983; Thunnissen *et al.*, 1990; White *et al.*, 1990). The NMR studies suggest that group I PLA_2s show significant

conformational differences in the 'interface recognition site' (IRS) of the free structure and the complexed structure. However, crystallographic studies demonstrate that as one of the most rigid proteins in nature, PLA_2s rarely show significant IRS conformational flexibility, suggesting that the substrate properties play the pivotal role in interfacial activity. In this paper, we report a crystal structure of a group II PLA_2 with remarkable conformational differences in a segment concerning the IRS. This crystallographic result favours the 'enzyme theory' of interface activation.

Four PLA_2s from the venom of the five-pace snake *D. acutus* (*A. acutus*) were obtained through gene engineering (Liu *et al.*, 2000). The amino-acid sequences of these PLA_2s were determined using the cDNA method (Liu *et al.*, 1999). They were designated acidic phospholipase A_2I (aPLA_2I), acidic phospholipase A_2II (aPLA_2II), basic phospholipase A_2 (bPLA_2) and Lys49-phospholipase A_2 (Lys49PLA_2) according to their isoelectric points, which are 4.49, 5.05, 9.49 and 9.3, respectively. aPLA_2I has an inhibitory effect on platelet aggregation, and all the phospholipase A_2s except aPLA_2II have haemolytic activities. aPLA_2I is the only known member of the acidic PLA_2s which exhibits haemolytic activity. An acidic PLA_2 recently purified from the venom of *D. acutus* and characterized by Zhang *et al.* (2000) also displays an inhibitory effect on platelet aggregation. In this paper, we report the crystal structure determination of this PLA_2 at 2.6 Å resolution and analyze the platelet site based on a comparison of the amino-acid sequences and the three-dimensional structures.

2. Materials and methods

2.1. Crystallization and data collection

The PLA_2 enzyme provided for crystallization was extracted from the venom of *D. acutus* (collected from Jiangxi Province, China) according to the procedure outlined previously (Zhang *et al.*, 2000). The enzyme showed significant catalytic activity. Crystals were grown at 291 K by the hanging-drop method with 10 mg ml^{-1} protein, 0.05 *M* HEPES buffer pH 7.5, 0.07 *M* NaCl and 12% MPD in 8 µl drops equilibrated against 0.5 ml of well solution consisting of 0.1 *M* HEPES buffer pH 7.5 and 70% MPD. Single crystals with dimensions of 0.10 × 0.15 × 0.25 mm were found in the drops after four weeks. The crystals belong to space group $P2_1$, with unit-cell parameters a = 48.71, b = 38.00, c = 69.90 Å, β = 99.35°. There are two protein molecules in the asymmetric unit. The crystal has a 46% estimated solvent content (V_M = 2.28 Å^3 Da^{-1}; Matthews, 1968). The detailed crystallization procedure and preliminary X-ray characterization of the crystal have been reported elsewhere (Zhang *et al.*, 2000).

Data were collected on a MAR 345 area detector (MAR Research; λ = 1.54178 Å) using a single crystal at a temperature of 293 K. The crystal-to-detector distance was 150 mm. The total rotation range φ was from 45 to 275° with an oscillation angle $\Delta\varphi$ of 1° and an exposure time of 540 s per frame. The data were scaled and merged using the *HKL* suite (Otwinowski & Minor, 1997). The data set has an R_{merge} of 12.2% and a completeness of 99.8% between 30 and 2.5 Å. The data-collection results are summarized in Table 1.

Table 1
Data-collection and structure-refinement statistics.

Data collection	
Resolution (Å)	2.5
No. of observations	80310
No. of unique reflections	8966
Completeness of data (%)	99.8 (100 for last shell)
$I/\sigma(I)$	14.1 (3.3 for 2.59–2.50 Å, 4.3 for 2.69–2.59 Å)
R_{merge} (%)	12.2 (40.3 for 2.59–2.50 Å, 33.5 for 2.69–2.59 Å)
Crystallographic refinement	
Resolution range (Å)	8.0–2.6
No. of reflections	7703
R factor (%)	18.40
R_{free} (%)	22.50
Model	
No. of non-H protein atoms	1923
No. of metal ions	3 (2 Ca^{2+}, 1 Zn^{2+})
No. of water molecules	94
R.m.s. deviations from ideal values	
Bond distances (Å)	0.007
Bond angles (°)	1.22
Dihedral angles (°)	23.88
Improper angles (°)	0.79

2.2. Structure determination and refinement

The structure was solved by the molecular-replacement method using the *CCP*4 suite (Collaborative Computational Project, Number 4, 1994). A 4 Å self-rotation function search using the *POLARRFN* program revealed a prominent peak (7.5σ) for χ = 180°, indicating the presence of a non-

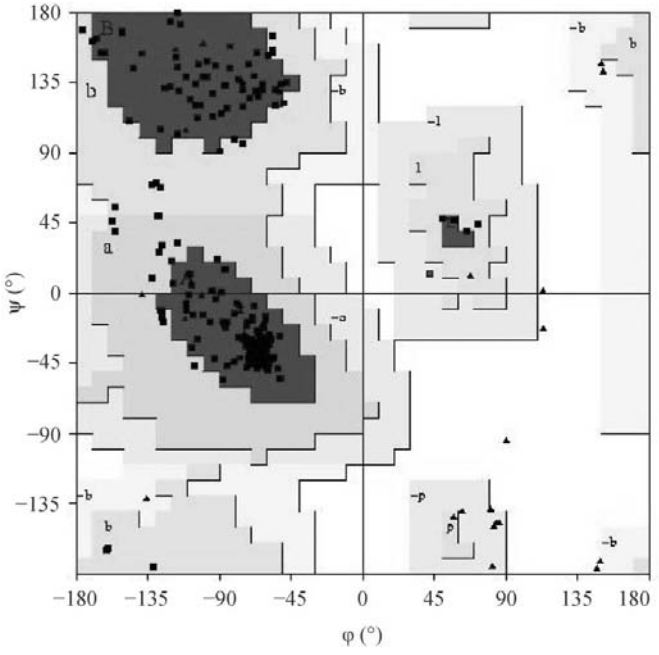

Figure 1
Ramachandran plot. 86.1% of residues are in the most favored regions (A, B, L; darkly shaded), 13.4% are in the additional allowed regions (a, b, l; shaded) and 0.5% are in the generously allowed regions (~a, ~b, ~l; lightly shaded). Glycine residues are shown as triangles.

crystallographic twofold symmetry axis, which is perpendicular to the *b* axis and deviates 13.1° from the *c* axis. It is assumed that the acidic PLA_2 enzyme studied here has the same sequence as the $aPLA_2I$ sequence deduced using the cDNA method (the $aPLA_2I$ sequence is hereafter called the reference sequence). The search model used in the cross-rotation function calculation was acidic PLA_2 from the venom of *A. halys pallas* (Wang, Yang *et al.*, 1996; PDB code 1psj), with a sequence identity of 70.2% compared with the reference sequence. All residues from the search model (124 in total) were used and the residues that differed between the two sequences were initially treated as alanines. The cross-rotation function search was calculated using the *AMoRe* program (Navaza, 1994) with data in the resolution range 8–4 Å and an integration radius of 19 Å. The top eight peaks of the cross-rotation function were used to calculate the translation functions. The translation function showed that the first and the third peaks were the correct solutions from their high correlation coefficients. The rigid-body refinement of *AMoRe* resulted in an *R* factor of 38.6% and a correlation value of 56.7%. The initial model, oriented and positioned according to the molecular-replacement solution, was examined on a Silicon Graphics O2 workstation using the program *FRODO*/*TURBO* (Jones, 1978). The molecular packing in the crystal was confirmed to be reasonable and consistent with the result of the self-rotation function.

The refinement was carried out using the *X-PLOR* program (Brünger, 1992*a*) followed by the *CNS* program (Brunger *et al.*, 1998), with 10% of the data reserved to calculate the free *R* factor (Brünger, 1992*b*). A total of 7703 reflections in the resolution range 8.0–2.6 Å were used in the refinement. The main chains and side chains of the molecules were adjusted according to the $2F_o - F_c$ and $F_o - F_c$ electron-density maps. Four inconsistencies in sequence were found at positions 102, 103, 131 and 133, where the electron density was not adequate for the side chains of the reference sequence. We changed these residues to Ala102, Ala103, Pro131 and Pro133, respectively. We also inserted a proline as residue 122 according to the electron-density map. These changes are consistent with the sequence of Taiwan *D. acutus* acidic PLA_2 deduced from the cDNA sequence (Wang, Wang *et al.*, 1996). Finally, two calcium ions, a zinc ion and 94 water molecules were included in the model based on their electron densities and environments. After several cycles of atomic position and *B*-factor refinements, the final *R* value fell to 18.40% with an $R_{\rm free}$ value of 22.50% in the resolution range 8.0–2.6 Å.

The final model has good stereochemical quality, with the r.m.s. deviations from ideal values being 0.007 Å for bond lengths and 1.22° for bond angles. The C^{α} r.m.s. differences calculated between the final model and the search model were 0.920 Å for molecule *A* and 1.515 Å for molecule *B*. Calculations using the program *PROCHECK* (Laskowski *et al.*, 1993) indicated that almost all non-glycine and non-proline residues in the asymmetric unit were located in the most favoured regions (173 residues) or the additional allowed regions (27 residues), with only one in the general allowed regions. The Ramachandran plot of the main-chain torsion angles (φ, ψ) (Ramachandran & Sasisekharan, 1968) showed that 86.1% of the residues were in the most favoured regions, with none of the residues in the disallowed regions (Fig. 1). The refinement results are listed in Table 1.

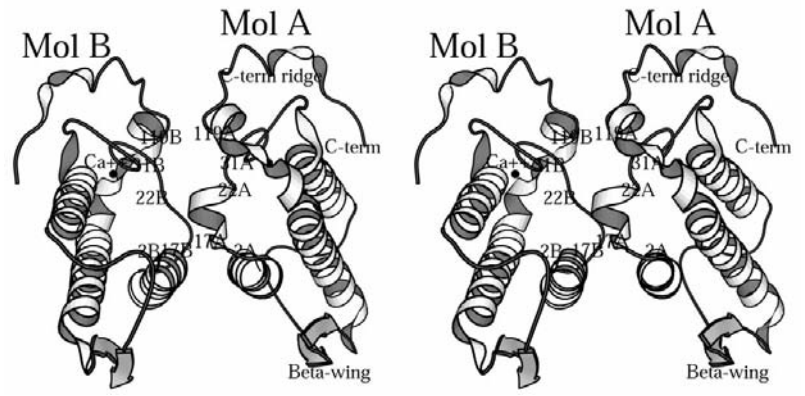

Figure 2
Ribbon digram of the dimer structure. The β-wing, C-terminus ridge, calcium ion and some residues at the interface are labelled.

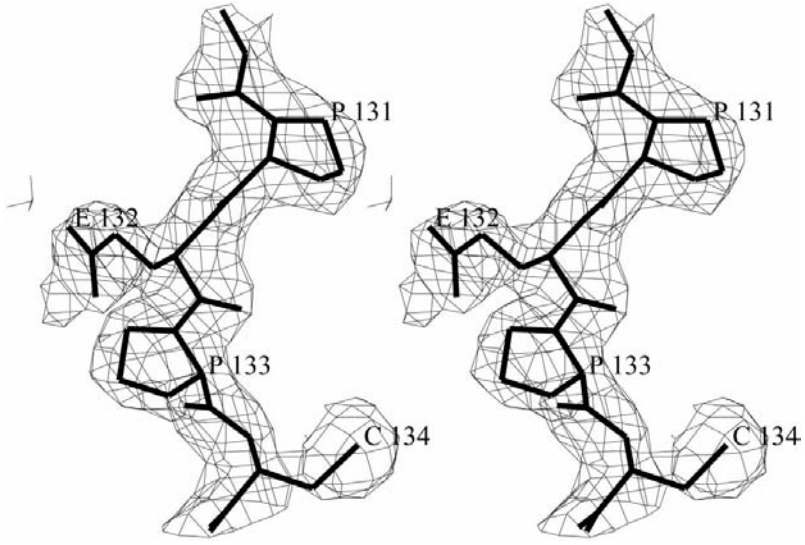

Figure 3
Stereoview of the omit $2F_o - F_c$ electron-density map contoured at the 1.0σ level showing the proline-rich C-terminus.

3. Results

3.1. Overall structure

The final model consisted of 1923 non-H protein atoms from two crystallographically independent molecules, two calcium ions, one zinc

ion and 94 water molecules. These atoms occupied 56.1% of the unit-cell volume. The $2F_o - F_c$ electron-density map is continuous and well defined for both the backbone and the side chains with the exception of a very small number of polar side chains on the molecule surface.

As a member of the group II PLA_2s (Heinrikson *et al.*, 1977; Dufton & Hider, 1983), *D. acutus* acidic PLA_2 has all the structural characteristics of this group of PLA_2. It contains three long α-helices, one double-stranded antiparallel β-sheet designated as a β-wing and a calcium-binding loop (Fig. 2). These structural elements as well as the C-terminal ridge are cross-linked by seven disulfide bonds. The structures of the active site and the hydrophobic channel are also highly conserved. The calcium ion binds at the highly conserved calcium-binding loop and the ligand O atoms form the usual distorted pentagonal bipyramidal structure. In this experiment, no calcium ions were added to the crystallization solutions; however, a strong electron-density peak at the expected calcium ion position around the calcium-binding loop indicated the presence of a calcium ion. Similar cases have been reported (see Wang, Yang *et al.* 1996).

The two molecules (*A* and *B*) in the asymmetric unit form a dimer with approximate twofold symmetry (Fig. 2). The dimer is stabilized by a large number of hydrophobic interactions and 12 direct or water-mediated hydrogen bonds. The surface area buried by the formation of the dimer is 983 Å^2 (*CCP*4; Collaborative Computational Project, Number 4, 1994), corresponding to 15.9% of the monomer surface area, a value close to that of a typical dimer (Janin *et al.*, 1988). Such dimers also exist in a novel crystal form (Gu *et al.*, unpublished results).

Although the crystallization solution did not contain any additional metal ions except for Na^+, the $F_o - F_c$ electron-density map displayed a significant isolated peak with $\sigma > 6$ near His34, indicating the presence of a second metal ion. This metal ion was coordinated by two histidine residues at position 34 from two adjacent dimers and two water molecules, with the ligands forming a distorted tetrahedral structure. The ligand chemistry suggests that the ion may be Zn^{2+}. It is not unusual for snake venom to contain minor amounts of metal ions including Zn^{2+} (Friederich & Tu, 1971). A similar Zn^{2+}-coordinated structure was reported in another protein from *D. acutus* venom, acutolysin-C, which was also crystallized in the absence of the additional Zn^{2+} ions (Zhu *et al.*, 1999).

In the final model, the residue sequence differs from the reference sequence (Liu *et al.*, 1999) at five positions. Three of these five differences involve prolines, thus forming a proline-rich C-terminus ridge (Fig. 3) as in the PLA_2 from the venom of *Crotalus atrox* (Brunie *et al.*, 1985). The difference between the X-ray sequence and the reference sequence implies that the reference sequence based on cloning of the PLA_2 may be derived from a mutant of the PLA_2 in the venom, which differs slightly from that isolated for this study. The X-ray sequence reported here is very similar to that of Taiwan *D. acutus* acidic PLA_2, with sequence differences of only 5.7%, indicating the proximity of *D. acutus* acidic PLA_2 from Jiangxi and Taiwan.

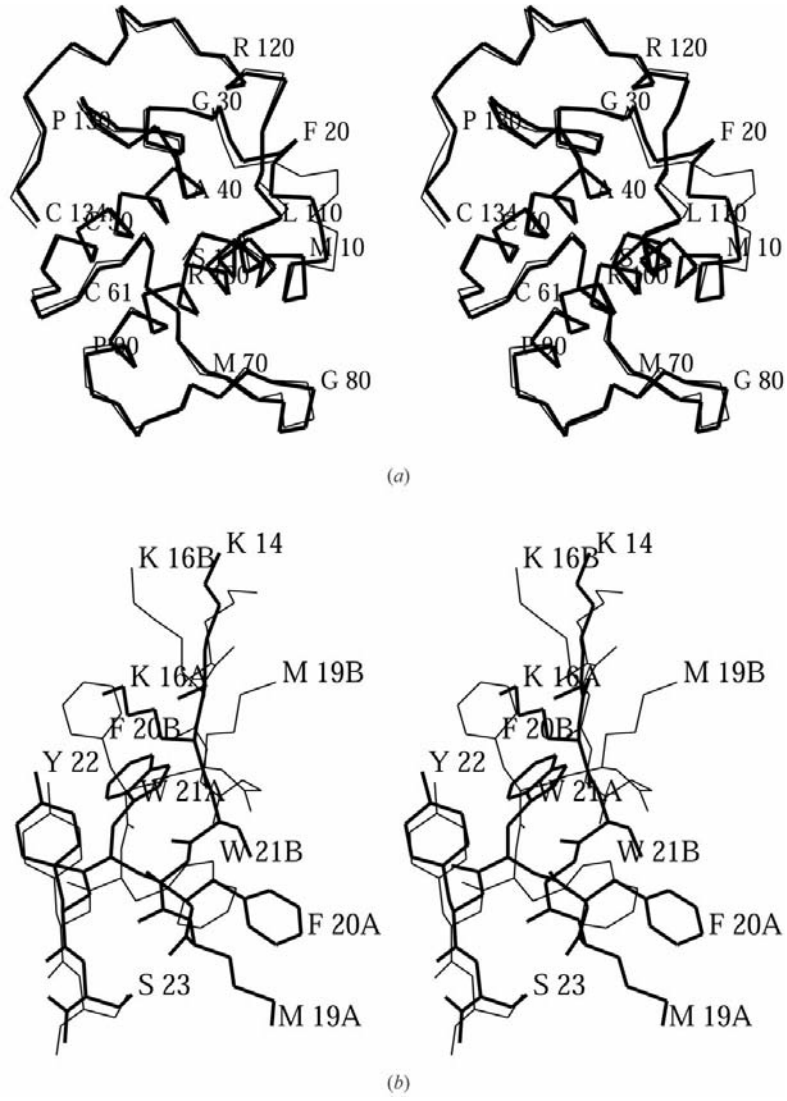

Figure 4
(*a*) Superposition of C^α traces of molecule *A* (thick line) and molecule *B* (thin lines). (*b*) Superposition of the segment 14–23 from molecule *A* (thick line) and molecule *B* (thin lines).

3.2. Local conformational adaptability

As a small protein containing seven disulfide bridges, the PLA_2 molecule shows resistance to denaturation (heat or hydrochloride guanidine; see Wu *et al.*, 1985; Scott, 1997) and conformational inflexibility. Usually, its conformations are affected little by its crystal environment. Unexpectedly, in this crystal structure the two molecules in the asymmetric unit greatly differ at the dimer interface (Figs. 2, 4*a* and 4*b*), where the structure is very

Table 2
Asymmetric hydrogen-bonding interactions at the dimer interface.

Atom in molecule *A*	Atom in molecule *B*	Distance (Å)
Glu6 OE2	Glu6 OE1	2.40
Ser17 OG	Glu6 OE2	2.37
Met19 N	Glu6 OE2	3.36
Met19 O	Ser23 OG	3.13
Phe20 O	Trp31 NE1	2.79
Arg120 NH2	Tyr121 O	2.73

reliable as shown by the well defined $2F_o - F_c$ electron-density maps (Figs. 5*a* and 5*b*). The superposition of the two molecules gives an r.m.s. deviation of 1.31 Å for all C^α atoms, in contrast to a value of 0.5 Å or less in normal cases. Fig. 6(*a*) shows the distances between equivalent C^α atoms after least-squares superposition of the two molecules. The greatest differences (>1.0 Å for the C^α atoms) are confined to three segments consisting of residues 14–23, 77–80 and 85–91, with the largest deviation at residue 19 (8.19 Å for its C^α atom). By omitting these three stretches of peptides from the superposition, the C^α atom r.m.s. deviation was reduced to 0.48 Å.

Segment 14–23 is located at the interface of the dimer (Fig. 2). This segment connects the first long α-helix and the calcium-binding loop. In molecule *A* the segment includes a short α-helix (17–22), while in molecule *B* it shows an irregular turn conformation. Structural comparison shows that in this region the conformation of molecule *A* is typical of PLA_2s, while that of molecule *B* is unusual. The breakdown of twofold symmetry at the interface results in asymmetrical hydrogen-bond interactions between the contact residues (Table 2). The conformation of segment 14–23 in molecule *B* is less stable than that in *A* as shown by its higher average crystallographic *B* factors (Fig. 6*b*) and fewer intramolecular hydrogen-bonding interactions compared with molecule *A* (seven hydrogen bonds in *A* but only four in *B*). A hypothetical dimer with strict twofold symmetry created using molecule *A* as a monomer had extensive short contacts at the dimer interface. To avoid the close contact, Trp21 was rotated about 180° around its C^α—C bond, leading to great changes in the course of the main chains and the orientation of the aromatic side chains of residues 20 and 21 and the hydrophobic side chain of Met19. Significant conformational changes extended as far as residue 16.

Normally, segment 14–23 contains a short α-helix as shown in molecule *A*. This work shows that the conformation of the segment can adapt on binding to a contacting molecule. This result is consistent with a recent NMR study of PLA_2 (Yuan *et al.*, 1999), which showed the absence of the short α-helix 17–22 in the solution structure. It is also consistent with a newly reported crystallographic study of bovine pancreatic PLA_2, in which the asymmetric unit contained a monomer and both the main chains and the side chains of residues 19–20 and 23–24 were wholly in double conformation (Steiner *et al.*, 2001).

The structure observed here suggests that the conformation of the segment in molecule *B* may resemble that in solution owing to the absence of the short α-helix. This is not unexpected, as the segment is marginally stabilized by the main-chain hydrogen bonds in the short α-helix (five residues long) and therefore its structure could change depending on the environment. Segment 14–23 together with the C-terminus ridge 110–134 involve a great number of residues at the IRS (Dijkstra *et al.*, 1981). The C-terminus ridge usually shows higher *B* factors relative to the

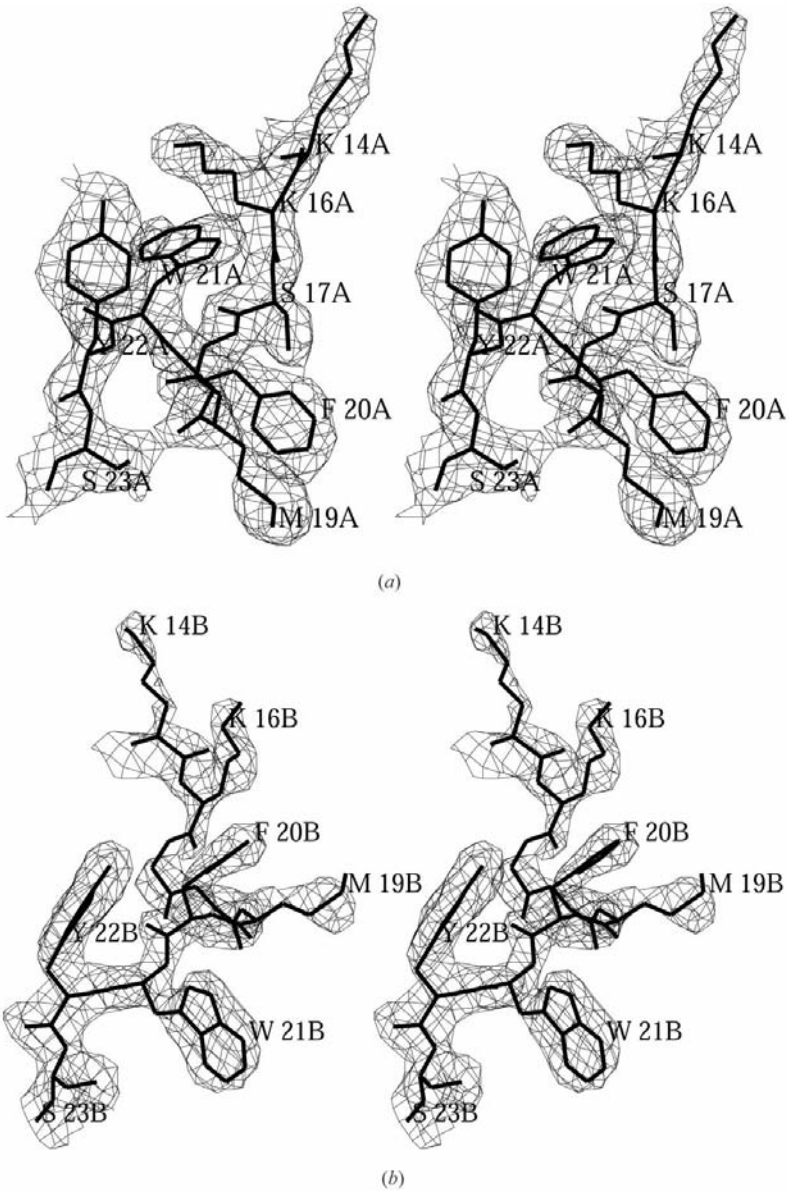

Figure 5
Stereoview of the $2F_o - F_c$ electron-density map contoured at the 1.0σ level showing the region around segment 14–23 of molecule *A* (*a*) and molecule *B* (*b*).

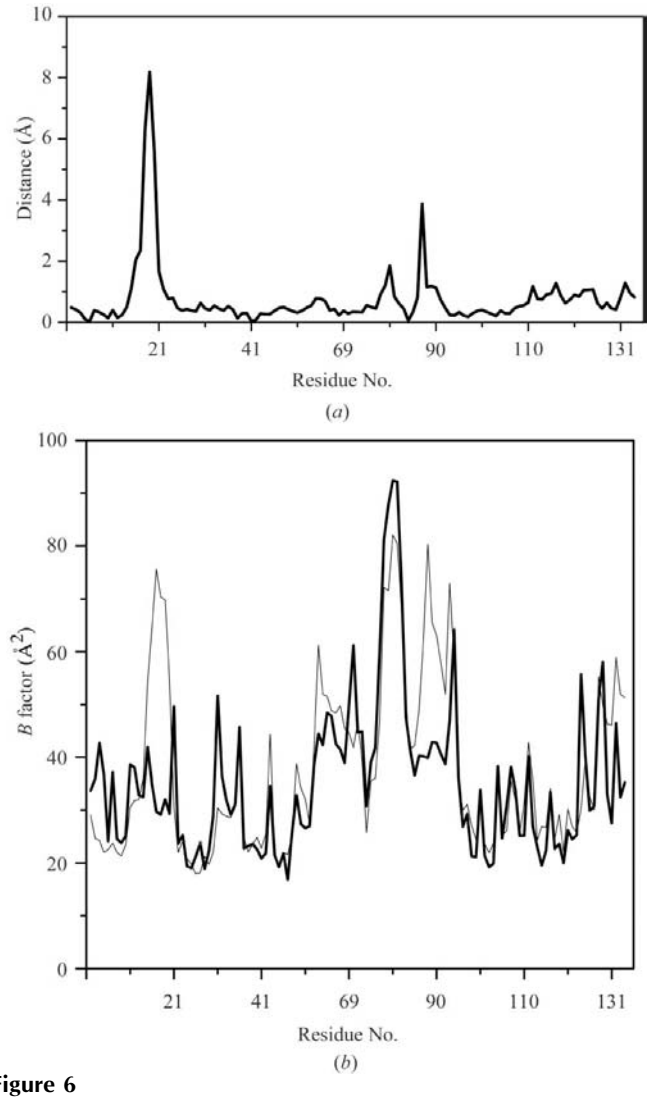

Figure 6
(*a*) Distances between C^{α} pairs of molecules *A* and *B* along the polypeptide chain. The average r.m.s. deviation for all the C^{α} pairs is 1.31 Å. The significant differences in segments 14–23 are clearly shown. (*b*) Plot of the temperature factor as a function of residue number for molecule *A* (thick line) and molecule *B* (thin line).

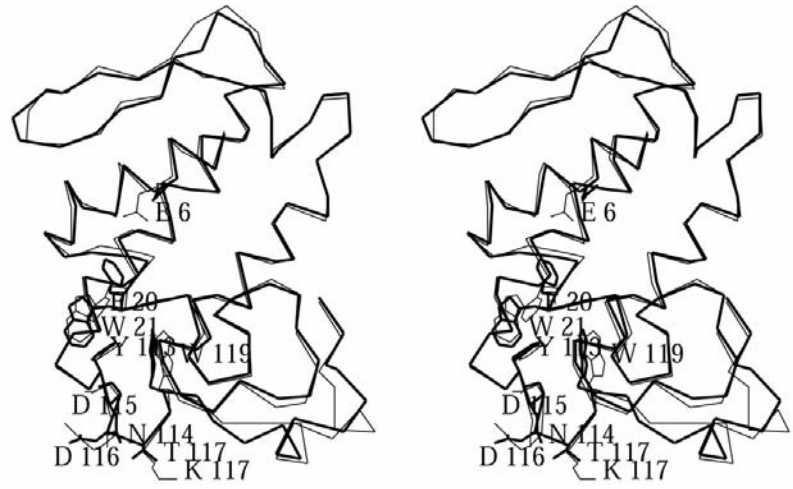

Figure 7
Comparison of the putative site responsible for inhibiting platelet aggregation. *D. acutus* $aPLA_2$ (thick lines) and *A. halys pallas* $aPLA_2$ (thin lines).

entire molecule in most PLA_2 crystal structures including the *D. acutus* $aPLA_2$ structure being reported here, which indicates its flexibility. Taken together with previous results for group I PLA_2s (Yuan *et al.*, 1999; Steiner *et al.*, 2001), we suggest that the flexibility of the IRS may be a common feature of PLA_2 and the 'allosteric activity' during the enzyme–oil/water interface interaction may require this flexibility.

In addition to segment 14–23, differences between the two independent molecules were also observed for segments 85–91 and 77–80. Segment 85–91 is a stretch of peptide connecting the β-wing and the third long α-helix. Least-squares superposition of the *A. halys pallas* $aPLA_2$ molecule onto both molecules *A* and *B* of *D. acutus* $aPLA_2$ resulted in deviations of the equivalent C^{α} atoms of this segment of less than 0.8 Å for *B*, but being much higher for *A*, with a largest deviation of more than 4.2 Å for the residue 86 C^{α} atom. Careful examination showed that this region in molecule *A* is in contact with a neighbouring molecule, while in molecule *B* it is exposed to the solvent environment. This suggests that the conformation of this region in molecule *B* is native (in fact, it is similar to other PLA_2s), while in molecule *A* it may be affected by interactions with other molecules. The segment 77–80 forms the tip of the β-wing, which is known to be flexible (Arni & Ward, 1996).

3.3. The putative antiplatelet site

The crystallography and site-directed mutation study of acidic PLA_2 from the venom of *A. halys pallas* suggested that an aromatic cluster (Phe20, Trp21, Phe113 and Trp119) and two acidic residues (Glu6 and Asp115) located on opposite sides of the cluster play important roles in the inhibition of platelet aggregation (Wang, Yang *et al.*, 1996; Liu *et al.*, 2001). Fig. 7 shows that *D. acutus* $aPLA_2$ also has the same aromatic cluster and Glu6 on one side as in *A. halys pallas* $aPLA_2$; however, the charge distribution on the other side of this cluster is different: the three charged residues Asp115, Lys116 and Lys117 are replaced by Ser115, Asp116 and Thr117. Biochemical research has indicated that *D. acutus* $aPLA_2$ also has an effect on platelet aggregation. Since Asp115 is indispensable for *A. halys pallas* $aPLA_2$ platelet aggregation activity and Asp116 in *D. acutus* $aPLA_2$ is in close proximity to Asp115, Asp116 in *D. acutus* $aPLA_2$ probably plays a similar role to that of Asp115. Therefore, the platelet aggregation inhibition site may be expanded to include residue 116.

Moreover, although both *A. halys pallas* $aPLA_2$ and *D. acutus* $aPLA_2$ affect platelet aggregation, their effects differ. The *A. halys pallas* $aPLA_2$ shows a class B effect on platelet aggregation, while the *D. acutus* $aPLA_2$ may belong to class C (Chen & Chen, 1989; Kini & Evans, 1997). It would be interesting to see if this classification has any relation to the special charge distribution around Asp116.

This work was supported by the Science Fund of the Chinese Academy of Sciences. We thank Dr Inn-Ho Tsai in Institute of Biological Chemistry, Academia Sinica, Taiwan for her most helpful discussion and Dr Xudong Zhao for his help during data collection and processing.

References

Arni, R. K. & Ward, R. J. (1996). *Toxicon*, **34**, 827–841.

Berg, B. van den, Tessari, M., Boelens, R., Dijkman, R., de Haas, G. H., Kaptein, R. & Verheij, H. M. (1995). *Nature Struct. Biol.* **2**, 402–406.

Berg, B. van den, Tessari, M., Boelens, R., Dijkman, R., Kaptein, R., de Haas, G. H. & Verheij, H. M. (1995). *J. Biomol. NMR*, **5**, 110–121.

Berg, B. van den, Tessari, M., de Haas, G. H., Verheij, H. M., Boelens, R. & Kaptein, R. (1995). *EMBO J.* **14**, 4123–4131.

Berg, O. G., Roger, J., Yu, B. Z., Yao, J. H., Romsted, L. S. & Jain, M. K. (1997). *Biochemistry*, **36**, 14512–14530.

Betzel, C., Genov, N., Rajashankar, K. R. & Singh, T. P. (1999). *Cell. Mol. Life Sci.* **56**, 384–397.

Brünger, A. T. (1992*a*). *X-PLOR v3.1 User's Guide. A System for X-ray Crystallography and NMR.* Yale University, New Haven, CT, USA.

Brünger, A. T. (1992*b*). *Nature (London)*, **355**, 472–475.

Brunger, A. T., Adams, P. D., Clore, G. M., DeLano, W. L., Gros, P., Grosse-Kunstleve, R. W., Jiang, J. S., Kuszewski, J., Nilges, M., Pannu, N. S., Read, R. J., Rice, L. M., Simonson, T. & Warren, G. L. (1998). *Acta Cryst.* D**54**, 905–921.

Brunie, S., Bolin, J., Gewirth, D. & Sigler, P. B. (1985). *J. Biol. Chem.* **260**, 9742–9745.

Chen, R. H. & Chen, Y. C. (1989). *Toxicon*, **27**, 675–682.

Collaborative Computational Project, Number 4 (1994). *Acta Cryst.* D**50**, 760–763.

Derewenda, Z. S. (1995). *Nature Struct. Biol.* **2**, 347–349.

Dijkstra, B. W., Drenth, J. & Kalk, K. H. (1981). *Nature (London)*, **289**, 604–606.

Dijkstra, B. W., Renetseder, R., Kalk, K. H., Hol, W. G. & Drenth, J. (1983). *J. Mol. Biol.* **168**, 163–179.

Dufton, M. J. & Hider, R. C. (1983). *Eur. J. Biochem.* **137**, 545–551.

Friederich, C. & Tu, A. T. (1971). *Biochem. Pharmacol.* **20**, 1549–1556.

Gowda, V. T., Schmidt, J. & Middlebrook, J. L. (1994). *Toxicon*, **32**, 665–673.

Heinrikson, R. L., Krueger, E. T. & Keim, P. S. (1977). *J. Biol. Chem.* **252**, 4913–4921.

Janin, J., Miller, S. & Chothia, C. (1988). *J. Mol. Biol.* **204**, 155–164.

Jerala, R., Almeida, P. F., Ye, Q., Biltonen, R. L. & Rule, G. S. (1996). *J. Biomol. NMR*, **7**, 107–120.

Jones, T. A. (1978). *J. Appl. Cryst.* **11**, 268–272.

Kini, R. M. & Evans, H. J. (1997). *Venom Phospholipase A_2 Enzymes: Structure, Function and Mechanism*, edited by R. M. Kini, pp. 369–387. Chichester: John Wiley & Sons.

Laskowski, R., Macarthur, M., Moss, D. & Thornton, J. (1993). *J. Appl. Cryst.* **26**, 283–290.

Liu, X. L., Pan, H., Yang, G. Z., Wu, X. F. & Zhou, Y. C. (1999). *Acta Biochim. Biophys. Sin.* **31**, 41–45.

Liu, X. L., Wu, X. F & Zhou, Y. C. (2001). *J. Nat. Toxins*, **10**, 43–55.

Liu, X. L., Xiong, Y., Wu, X. F. & Zhou, Y. C. (2000). *Protein Pept. Lett.* **7**, 83–90.

Matthews, B. W. (1968). *J. Mol. Biol.* **33**, 491–497.

Navaza, J. (1994). *Acta Cryst.* A**50**, 157–163.

Otwinowski, Z. & Minor, W. (1997). *Methods Enzymol.* **276**, 307–326.

Peters, G. H., Toxvaerd, S., Larsen, N. B., Bjornholm, T., Schaumburg, K. & Kjaer, K. (1995). *Nature Struct. Biol.* **2**, 395–401.

Ramachandran, G. N. & Sasisekharan, V. (1968). *Adv. Protein Chem.* **23**, 283–438.

Scott, D. L. (1997). *Venom Phospholipase A_2 Enzymes: Structure, Function and Mechanism*, edited by R. M. Kini, pp. 97–128. Chichester: John Wiley & Sons.

Scott, D. L., Otwinowski, Z., Gelb, M. H. & Sigler, P. B. (1990). *Science*, **250**, 1563–1566.

Scott, D. L., White, S. P., Otwinowski, Z., Yuan, W., Gelb, M. H. & Sigler, P. B. (1990). *Science*, **250**, 1541–1546.

Steiner, R. A., Rozeboom, H. J., de Vries, A., Kalk, K. H., Murshudov, G. N., Wilson, K. S. & Dijkstra, B. W. (2001). *Acta Cryst.* D**57**, 516–526.

Thunnissen, M. M., Ab, E., Kalk, K. H., Drenth, J., Dijkstra, B. W., Kuipers, O. P., Dijkman, R., de Haas, G. H. & Verheij, H. M. (1990). *Nature (London)*, **347**, 689–691.

Wang, X. Q., Yang, J., Gui, L. L., Lin, Z. J., Chen, Y. C. & Zhou, Y. C. (1996). *J. Mol. Biol.* **255**, 669–676.

Wang, Y. M., Wang, J. H. & Tsai, I. H. (1996). *Toxicon*, **34**, 1191–1196.

Wells, M. A. (1974). *Biochemistry*, **13**, 2248–2257.

White, S. P., Scott, D. L., Otwinowski, Z., Gelb, M. H. & Sigler, P. B. (1990). *Science*, **250**, 1560–1563.

Wu, X. F., Shi, Q. L., Chen, Y. C. & Lu, Z. X. (1985). *Acta Biochim. Biophys. Sin.* **17**, 507–513.

Yuan, C., Byeon, I. L., Li, Y. & Tsai, M. D. (1999). *Biochemistry*, **38**, 2909–2918.

Zhang, H. L., Lin, Z. J., Du, X. Y. & Zhou, Y. C. (2000). *Acta Biochim. Biophys. Sin.* **32**, 337–341.

Zhu, X. Y., Teng, M. K. & Niu, L. W. (1999). *Acta Cryst.* D**55**, 1834–1841.